Flammability studies for wildland and wildland-urban interface fires applied to pine needles and solid polymers

FLAMMABILITY STUDIES FOR WILDLAND AND WILDLAND-URBAN INTERFACE FIRES APPLIED TO PINE NEEDLES AND SOLID POLYMERS

A. Simeoni[a], J.C. Thomas[a], P. Bartoli[b,c], P. Borowieck[b], P. Reszka[b], F. Colella[d], P.A. Santoni[c] and J.L. Torero[b]
asimeoni@wpi.edu
[a] Department of Fire Protection Engineering, Worcester Polytechnic Institute, USA
[b] BRE Center for Fire Safety Engineering, University of Edinburgh, UK
[c] UMR CNRS SPE 6134, University of Corsica, France
[d] Dipartimento di Energetica, Politecnico di Torino, Italy

Abstract
This paper presents flammability studies related to wildland fires that have been conducted at the University of Edinburgh and at WPI over the last 5 years. This is the first time that all of the contributions have been put together to present a consistent set of studies geared towards a better understanding of how wildland and solid fuels ignite and burn in the context of wildland and wildland-urban interface fires. The whole approach is based on experiments conducted with the Fire Propagation Apparatus. This experimental device was used due to its versatility, allowing for testing over a wide range of conditions applied to different forest fuels. To simplify the approach, well-characterized fuels were used in the form of dead pine needles and solid polymers. The different sets of results show that this approach enhances our understanding of wildland fire behavior and impact in general but also, more specifically, at the wildland-urban interface. These experimental data, along with the models developed to describe ignition, represent a successful application and extension of approaches and techniques developed for fire safety studies to the topic of wildland fires.

Keywords: Wildland fires, wildland fuels, flammability, Fire Propagation Apparatus, time to ignition, structural ignition, heat release rate.

1. Introduction
Wildland fires represent a growing threat to human infrastructure and activities due to both climate change and the spreading of the Wildland-Urban Interface (WUI). More than ever, wildland fire professionals need to understand how wildland fuels and structural materials ignite and burn at the WUI. To help manage the increasing risks and better develop wildland management solutions, improved assessment tools need to be developed.

One of the main factors that influences fire spread is wind, which provides fresh oxygen to the fuel and also alters the flame shape, thereby influencing the preheating of the unburned fuel. Another key element, which is also influential to the burning behavior, is the fuel being consumed. Its geometrical, physical and chemical properties have an impact on the fire that needs to be evaluated. These two factors have been extensively studied and integrated in the development of statistical [1] or empirical [2] fire-spread models. Though these models have made a significant contribution to our ability to manage wildland fires, the complexity associated with the highly porous fuels making up vegetation demands that researchers return to first principles. Generating a better understanding of the way in which the flow through the fuel layer affects ignition and combustion processes, as well as how fuels differ in their burning dynamics, is an essential task that needs to be examined in a systematic manner.

Simple fire-spread models do not describe combustion. To compensate, the influence of wind on the fire is represented by a correction factor for the rate of spread [2] but such models are unable to reproduce the full coupling between the fire and the atmosphere [3]. Detailed physical models [4-6], which are based on Computational Fluid Dynamics, describe the physics involved in fire spread in great detail. However, they are not able to successfully couple the flow-field with the burning behavior because the influence of the flow on the ignition and burning of vegetation is not fully described in the sub-models. All the model limitations cited above are mainly due to limited research on the burning dynamics of vegetation. Improving these models (such as WFDS, which is specifically dedicated to the WUI problem, [5, 7]) will lead to an improved description of fire at the WUI. A systematic investigation on the burning dynamics of vegetation is thus necessary to alleviate a primary bottleneck in wildland fire research that limits the use of detailed models beyond research tools [8]. This statement can be extended to the development of risk indexes, which describes potential forest fire danger in a region. The system currently in use in the U.S.A. is the National Fire Danger Rating System (NFDRS) [9, 10]. The fire behavior properties used to define the risk are the Rate of Spread (ROS) and the heat released per unit area. These two factors are estimated based on Rothermel's semi-empirical model [2] and empirical data [9]. Other risk indexes [11-13] are based on considerations similar to NFDRS, but they use empirical formulas for the ROS and a rough evaluation of the heat released, which is called the Fire-Line Intensity and is defined as the heat released per meter of fire front [14].

The flammability is usually defined by the Time to Ignition (TI), the Heat Release Rate (HRR) and the ROS [15, 16]. The flammability of solid fuels has been extensively studied [17], but this is not the case for wildland fuels [18]. Wildland fuels are very different from the usual fuels encountered in human-developed environments. They are extremely porous, with porosities ranging from 0.05 for pine needle litters to 0.002 for tree canopies [19, 20]. The influence of the physical and geometrical properties of the fuel, as well as the bulk properties of the fuel layers was often neglected because the protocol did not focus on them [21, 22]. Usually, simple protocols are used to estimate the three quantities, but they do not relate to the fundamentals of the phenomena. TI is estimated by putting fuel samples under a radiant heater [23]. The Heating Value measured in a bomb calorimeter is generally used instead of the HRR [24]. ROS has been extensively studied at the laboratory scale [25, 26]. Even if the relevance of these studies to fires in the field needs to be thoroughly investigated, the aspects of flammability that need to be examined in more detail in the laboratory are TI and HRR. In the past, a small number of studies were conducted using the cone calorimeter [27, 28], but they mainly focused on classifying fuels.

Another acute problem at the WUI is structural ignition. In this case, the primary parameter is TI because the structure will be considered to be lost if ignited and not defended by fire-fighting means. The fuels of interest in this scenario are solid and located on the external envelope of the structure. Wildfires approaching the WUI induce time-varying incident heat fluxes, which render the classical solutions developed for constant heat fluxes [29] inaccurate. In this case, studies for time-varying incident heat fluxes need to be developed.

This paper presents the flammability studies developed at the University of Edinburgh and at WPI that were dedicated to the understanding of the parameters affecting fuel flammability. Both the approach and the developed models were based on experiments conducted with the Fire Propagation Apparatus. This experimental device was used due to its versatility, allowing for testing over a wide range of conditions applied to different fuels. The combined influence

of conditions and fuel type on TI and HRR was investigated. Some bulk properties of wildland fuels, such as radiation attenuation and permeability were also determined experimentally in this study to understand the coupling between the fuel burning and the flow.

Regarding TI, two approaches were adopted. The first one was dedicated to wildland fuels and to understand their conditions of ignition when submitted to various radiant heat fluxes and flow conditions. The classical approach was used in the FPA with constant heat fluxes, but adapted sample holders were used to permit the flow to go through the sample, thus allowing the study of its influence on TI. Fundamentally, this study can be related to the influence of wind on the ignition of porous wildland fuels. A model was developed to better understand this influence and the influence of the different fuel properties on the ignition process. The second approach was dedicated to solid materials. Ramping heat fluxes were used to represent the effect of an approaching fire in the context of the WUI. The objective of this study was to provide a mechanism to assess the potential for ignition while not adding an excessive computational burden to fire-spread models. This is particularly important for CFD fire spread models. These models focus on describing the fire spread through the fuel beds, and adding the full description of the interaction between the fire and the structure would be too computationally costly because of the wide range of time and length scales involved [3, 30]. To avoid resolving the building, the objective is to extract information from the CFD model that can then be used directly to establish if the material has ignited or not without requiring the modeling of the solid fuel itself. This approach imposes strong simplifications that will be argued hereafter on the basis of analytical formulations and experiments.

Concerning the HRR, only wildland fuels were used to investigate the influence of flow on burning dynamics. The role of permeability was investigated, as well as the effects of changing the fuel species under the same flow conditions. Only experimental studies were conducted, and modeling has yet to develop that takes into account the influence of flow through the porous fuel on the behavior of the condensed phase and particularly on pyrolysis and char combustion.

Ideal fuels were used in the form of dead pine needles to represent wildland fuels and polymers to represent solid fuels. Pine needles were used for both TI and HRR studies and polymers only for TI. The pine needles and polymers that were used are well characterized and have been extensively studied in wildland fire and fire safety research, respectively. These fuels allowed focusing the study on the parameters mentioned above without adding the uncertainties related to poorly characterized fuels. However, the approach to studying flammability presented in this paper is proposed as a general method that can be applied to other wildland and solid fuels in the context of wildland and WUI fires.

The effect of moisture content of vegetation and embers are not covered here but interested readers are referred to [31] and the paper dedicated to firebrands in the same journal issue as this paper [32], respectively.

Section 2 presents the experimental protocols developed for FPA studies as well as the experiments dedicated to the measurement of the radiation attenuation and the permeability of pine needle beds. Section 3 presents the studies related to TI. The first subsection is dedicated to the pine needle experiments and the second one is dedicated to solid fuel experiments. Section 4 is dedicated to the HRR studies, with a subsection on flow and fuel property effects, respectively.

2. Experimental Apparatuses and Methods

2.1. Fire Propagation Apparatus

The FM-Global Fire Propagation Apparatus (FPA) was used to conduct the test series presented in this paper [33]. Its basic layout is presented in Fig. 1. The FPA operates on a similar concept to a cone calorimeter. A fuel sample is subjected to a radiative heat flux and an ignition source is provided by the use of an ethylene/air pilot flame. The mass loss rate of the sample is measured and the exhaust gases are analyzed for composition, temperature, optical obscuration, and pressure drop across an orifice plate. One key difference with the FPA in comparison to the cone calorimeter is that the combustion chamber for the sample allows for a controlled environment with respect to gas flow rate and composition.

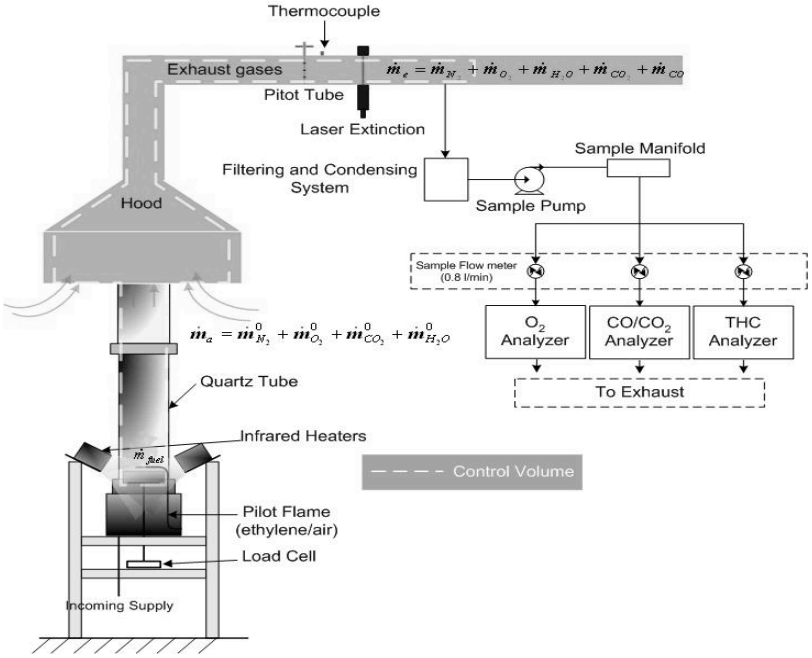

Figure 1. Overview of the FPA.

The combustion chamber and the sample holder for the FPA are cylindrical. The sample holder fits inside the combustion chamber and is positioned on a balance. Different experimental factors were tested. Table 1 summarizes the experimental conditions related to the different sections of the paper. Detailed parts of the protocol specific to each series of tests are presented in each section.

Custom-made sample holders were designed for testing porous wildland fuels and are depicted in Fig. 2. Their dimensions were 126 mm in diameter and 31 mm in depth (Table 1). They were made of stainless steel and had a uniform pattern of small holes in all (side and bottom) of their outside surfaces. These holes created an open space allowing air to pass into the holders and through the fuel samples. The basket opening is defined as the percentage of open surface of the baskets (see figures 2.a and b for the open baskets and Table 1 for the used values). Some other tests also used baskets lined with aluminum foil to prevent flow to go through the fuel bed. The different basket opening allowed testing different airflows at both natural convection and forced airflow conditions. The flow was allowed to fully establish before applying the heat flux. The baskets were filled to the top and had masses from 10 to 20 g (Table 1).

For solid fuels, ignition tests with in-depth temperature measurements have been carried out on 110 x 110 x 12 mm samples of pure PA6 (Nylon 6), and of PA6 with nano-composites (Table 1). Small holes have been drilled through the samples for thermocouple measurements [30]. The tested material was pasted to an aluminum block of same surface area and 24 mm thickness and insulated on the sides. Ignition tests were also performed using PMMA samples of dimensions 100 x 100 x 4.9 mm. No temperature measurements were carried out for this last material. Some fuels filled with nano-composite retardants were also tested to investigate if these components were changing the fuel behavior or just delaying it.

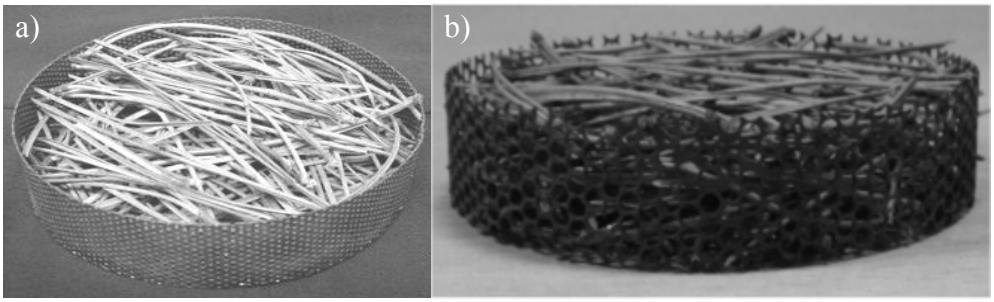

Figure 2. Sample baskets filled with *Pinus pinaster* a) 26% b) 63% open basket.

Table 1. Experimental design.

Section	Fuel species	Basket opening (%)	Sample size (mm)	Mass (g)	Heat Flux	Flow (l/mn)
3.3	*Pinus halepensis and Pinus strobus*	0, 63	126 (diameter) x 31 (height)	15	8.5 to 60 kW/m^2	0, 50, 100, 200
3.4	PA6, PA6+NC, and PMMA*	0	110 x 110 x 12 (PA6/NC) 110 x 110 x 4.9 (PMMA)	70, 170	0.01-5.0 kW/m^2 s	0
4.1	*Pinus pinaster* and *Pinus halepensis*	0, 26, 63	126 (diameter) x 31 (height)	15	25 kW/m^2	0, 200
4.2	*Pinus pinaster*, *Pinus halepensis,* and *Pinus laricio*	0, 63	126 (diameter) x 31 (height)	10-20	25 kW/m^2	0, 100, 200

** PA6 is Nylon 6, PA6+NC is Nylon 6 with nano-composites and PMMA is Polymethylmethacrylate*

The interest in using a radiative insult for wildland fire studies is that small samples can be submitted to high radiative fluxes, in the order of magnitude of the fluxes encountered in the field. For ignition studies, the radiative heat flux imposed on the sample was between 8.5 and 60 $kW.m^{-2}$ (Table 1), as this range of values is characteristic of surface fires in pine needle beds [34]. As opposed to the TI studies, the heat flux was set to 25 $kW.m^{-2}$ for the HRR studies. This value was selected because it allowed ignition times and flame durations to be obtained, which were suitable for the comparison between the various experimental conditions, while remaining in the lower range of encountered heat fluxes.

2.2. Characterization of the fuel

Four forest fuels and three solid fuels were studied in the different test series (see Table 1). *Pinus pinaster*, *Pinus laricio* (subspecies of *Pinus nigra*) and *Pinus halepensis* needles were collected from Mediterranean wildland areas. *Pinus strobus* needles were collected from Massachusetts, USA. Each species was collected at the same location and during the same season for the whole sets of experiments. The needles were dead and not conditioned prior to

testing. The moisture levels of the needles were determined by oven drying of a sample for 24 hours at 60 ºC. The moisture content of the samples ranged from 5 to 8% on a dry basis. The surface-to-volume ratios were σ_s = 3,057 m^{-1}, 4,360 m^{-1}, 7,377 m^{-1}, and 10,788 m^{-1} for *Pinus pinaster*, *Pinus laricio*, *Pinus halepensis*, and *Pinus strobus*, respectively, with an approximate 3% error [35, 36]. As the volume of the samples was kept constant (volume of the holders), the bulk densities were 25.87, 38.81, and 51.74 kg/m^3 for 10, 15, and 20 g samples, respectively, independent of the species.

The three solid fuels were Nylon 6 (PA6), Nylon 6 with nano-composites (PA6+NC) – the nano-composites being ceramic nano fillers – and polymethylmethacrylate (PMMA). The nano-composites were added to study the influence of this flammability control strategy on fuel flammability.

The time to ignition of all these porous and solid fuels has been extensively studied, providing a good background to study the effect of other parameters, such as flow or time-varying radiant heat fluxes. This prevents adding the uncertainties associated with poorly characterized fuels to the analysis of the results.

2.3. Radiation Attenuation

A specific device has been developed to measure the radiation attenuation coefficient of the fuel bed, which plays a prevalent role for the ignition of porous fuels submitted to radiant heat fluxes. This coefficient is one of the main bulk properties of the fuel beds that differ greatly from solid fuels [37]. Figure 3a shows the experimental apparatus. It consisted of a cylinder, adjustable in height, placed over a circular plate. A Medtherm® heat flux meter was inserted in a hole at the center of the plate. The inner sides of the cylinder were painted black. A cone heater was located above the cylinder, providing a constant heat flux at the top of the fuel bed. A shield was positioned between the cone heater and the sample to allow a sudden exposure to the constant heat flux when removed. Each exposure lasted for approximately 8 seconds in order to avoid pyrolysis, twisting of the needles, and re-radiation from the sides of the cylinder to occur. The bulk density of the fuel samples was set to match the FPA experimental conditions.

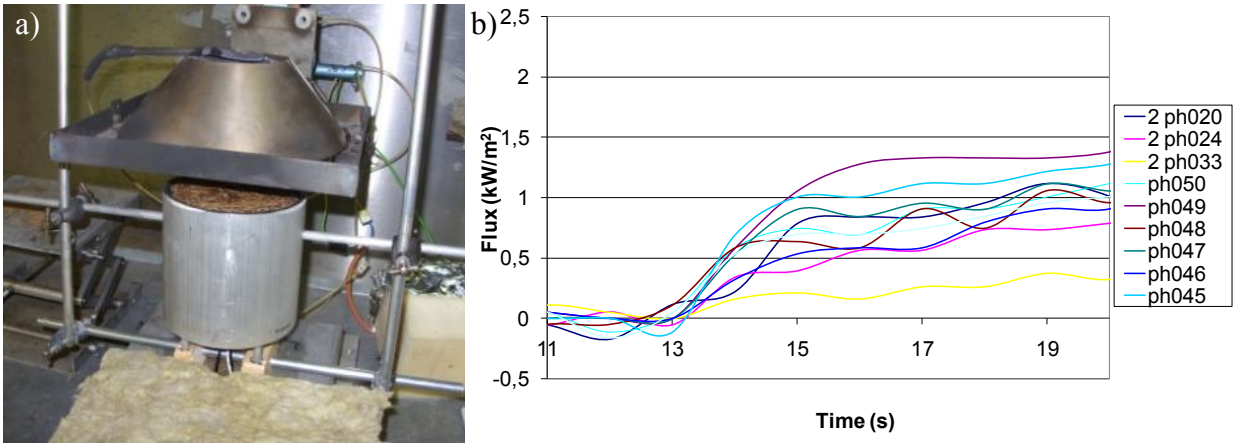

Figure 3. a) Radiation attenuation device b) Heat flux measured at the bottom of the fuel bed for a constant radiant heat flux of 30 kW/m^2 at the top of the fuel bed and a fuel bed depth of 2 cm. The legend corresponds to different repetitions.

Grishin et al. [38] found that radiation attenuation in pine needle beds follow the Beer-Lambert law. Thus, it was applied to determine the radiation attenuation coefficient of one fuel bed made of *Pinus halepensis* needles with the following properties [39]: $\rho_s = 789$ kg/m^3 (density), $\rho_s^* = 38.81$ kg/m^3 (bulk density), $\sigma_s = 7377$ m^{-1} (surface-to-volume ratio), and $\alpha_g = 0.9508$ (porosity). The ignition models presented in sections 3.2 have been applied to the exact same conditions.

Several repetitions were carried out, changing the geometrical arrangement of the pine needles in the samples. The results are shown in Fig. 3b. They are quite scattered because of the combination of the small surface of the heat flux meter used to measure the heat flux and the random positioning of the pine needles. An average value of the attenuated flux has been chosen to be 1 kW/m^2, leading to a value of $K = 170$ m^{-1} and a path length $d = 1/K = 5.88$ mm. If one uses the classical relationship $K = \alpha_k \sigma_k / 4$ [40] (with α_k being the fuel volume fraction and σ_k being the fuel surface-to-volume ratio) and the geometrical properties of the fuel to estimate the attenuation coefficient, the obtained value is: $K = 91$ m^{-1}. Thus, the attenuation commonly used in models [4, 41] is strongly underestimated in the case of pine needle beds. One possible explanation is that the classical relationship is based on the hypothesis of an isotropic medium [40], which is not realistic for forest fuel layers with pine needles that are mainly horizontally orientated. The value obtained with this set-up is even higher than the value obtained by measuring attenuation of visible light [42], which already showed a discrepancy with the theory.

2.4. Permeability

The interaction between the solid fuel and the gas flowing through the porous fuel is represented by the bed permeability, as long as the flow is laminar. This quantity depends on many fuel properties, such as the surface-to-volume ratio, the roughness of the particle's surface and the fuel bed porosity, among others. There is no simple relationship between permeability and one of these properties taken alone [43]. Permeability (or drag forces for turbulent flows) can be included as model parameters to describe the gas/solid interaction in detailed physical models [37, 44].

The permeability of forest fuel beds has been estimated for *Pinus pinaster*, *Pinus laricio* and *Pinus halepensis*, and for different compactness. A simple and robust experiment has been designed [35], composed of an electric fan, a contraction chamber, and a work module with a total length of 800 mm (see Fig 4a). Static pressure taps were connected along the length of the tube at regular intervals. A hotwire anemometer was used to measure the exit velocity of the airflow.

The values of permeability have been determined using Darcy's law for low flow velocities that ranged between 0.2 m.s^{-1} and 1 m.s^{-1}. These velocities correspond to a laminar flow through the pine needles and the experimental results displayed a linear relationship between pressure drop and flow velocity (see Fig. 4b). The experimental set-up did not allow measuring the permeability for *Pinus halepensis* beds with a low compactness since the needles were collapsing in the tube to higher compactness. For the compactness that was too low to allow the value of the permeability to be measured, it was extrapolated from the permeability obtained with denser fuels.

The results for the permeability experiments are given in Table 2. The fuel bed permeability depends on the compactness of the bed. Indeed, it decreases with the mass of the fuel sample used in the calorimetry experiments as all the fuel samples have the same volume. It also

depends on the other geometrical (surface-to-volume ratio and shape) and physical (density and roughness) properties of the pine needles, and the same volume fraction will not provide the same permeability for different fuel species.

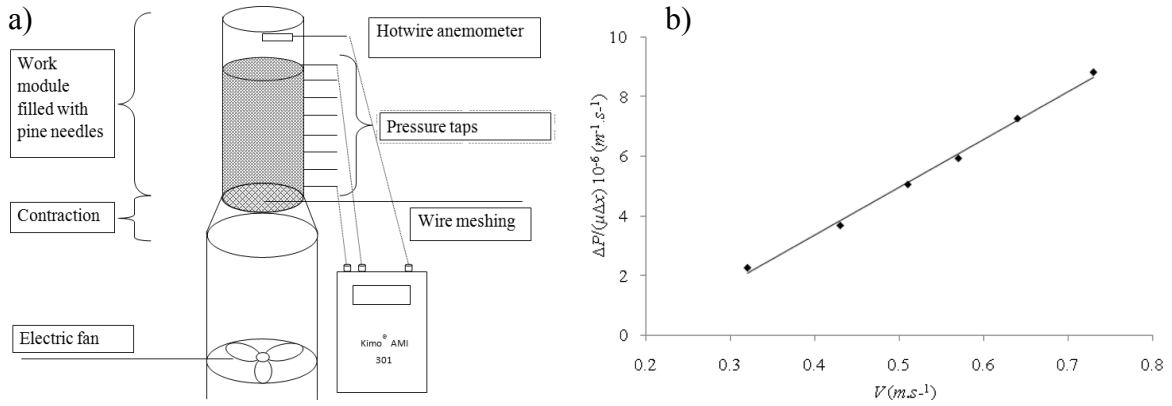

Figure 4. a) Layout of the permeability experimental setup. b) *Pinus halepensis* pressure drop per unit length as a function of flow velocity for a fuel load equivalent to a 20 g sample.

Experimental results for *Pinus halepensis* and a load equivalent to a 20 g sample in the calorimetry experiments (see section 4.2) are given as an example in Fig. 4b. The pressure drop inside the porous fuel bed is proportional to the imposed flow velocity. The permeability K is then deduced from the slope.

Table 2. Permeability (10^{-7} m^2) of samples for the three pine species and the different mass values used in the calorimetry experiments.

Sample mass (g)	**10**	**15**	**20**	**25**
Pinus halepensis	-	0.906	0.571	0.303
Pinus pinaster	2.649	1.014	0.640	0.397
Pinus laricio	3.144	1.447	0.892	0.448

3. Time to Ignition

The TI studies are presented in two sections. The first section presents the results on dead pine needle beds. It is divided between the presentation of the modeling approach and the results and discussion. The modeling approach tested a model developed for a solid fuel subjected to constant heat fluxes [49, 50], and a new model was developed to take into account the porous aspect of the fuel. The second section presents the experimental study of the ignition of solid polymers submitted to time-varying heat fluxes. Only piloted ignition was studied because it was assumed that the ignition source is the fire front itself for a spreading fire.

3.1. Pine Needle Beds

Two series of tests have been conducted, one for *Pinus halepensis* and another one for *Pinus strobus* (Table 1). Experimental results from [39, 47, 48] (*Pinus halepensis*) and original experiments (*Pinus strobus*) have been used, representing over 120 experiments. Sample holders with 0 and 63% openings have been used. The sample holders were filled to the top and had a constant mass of 15 g with a fuel bed porosity about 95%. The pine needles

completely shaded the basket, despite the high value of porosity, because the needles have a high surface-to-volume ratio and a sickle-shaped cross-sectional area.

A thermocouple (250 µm, K-type) was placed to measure the temperature at the top of the samples for *Pinus strobus* and a custom-made blockage device was placed into the FPA's test chamber just underneath the sample holder. This device blocked the airflow around the sample, forcing all the flow to go through it, whereas for *Pinus halepensis*, air could pass on the basket side rather than flowing through it [49]. The blockage device was used only for these more recent experiments to obtain more well-defined flow conditions. For *Pinus halepensis*, the radiative heat flux imposed at the top of the samples ranged from 8.5 to 50 kW/m^2 and for *Pinus strobus*, it ranged from 20 to 60 kW/m^2.

3.2. Ignition models

a) Solid Fuel Model

As the complete description of the model can be found in [46], only a simple description will be provided in the following. The model describes the heating process of a thermally-thick and semi-infinite solid fuel by the following energy equation and boundary conditions [45]:

$$\frac{\partial^2 T}{\partial x^2} = \frac{1}{\alpha_T}\frac{\partial T}{\partial t}, \qquad x = 0,\ -k\frac{\partial T}{\partial x} = \dot{q}''_S(0,t),\ \begin{matrix} t = 0 \\ x \to \infty \end{matrix} \quad T = T_\infty \tag{1}$$

where T is the temperature, α_T is the thermal diffusivity, k is the thermal conductivity and $\dot{q}''_S(0,t)$ is the net heat flux at the surface of the sample. This flux is a function of the external heat flux and the heat transfer with the ambient:

$$\dot{q}''_S(0,t) = a\dot{q}''_e - h_T(T(0,t) - T_\infty) \tag{2}$$

where a is the absorptivity of the fuel, $\dot{q}''_e$ is the external heat flux received at the surface of the solid and h_T is the total heat transfer coefficient, including the convective and radiative heat transfers.

By non-dimensionalizing all variables in the following way:

$$\overline{T} = \frac{T - T_\infty}{T_{ig} - T_\infty}, \quad \overline{x} = \frac{x}{x_c}, \quad \overline{t} = \frac{t}{t_c}, \quad \overline{\dot{q}}'' = \frac{\dot{q}''}{\dot{q}''_c} \tag{3}$$

where $x_c = k/h_T$, $t_c = k\rho C_p / h_T^2$, $\dot{q}''_c = h_T\left(T_{ig} - T_\infty\right)/a$.

The following solution is obtained for the evolution of the temperature at the surface of the solid [46]:

$$\overline{T}_S = \overline{\dot{q}}''_e\left[1 - e^{\overline{t}}\,\mathrm{erfc}(\sqrt{\overline{t}}\,)\right] \tag{4}$$

To solve for the ignition time ($\overline{t}_{ig}$), a first order Taylor series expansion of Eq. (4) is conducted [46]. The range of validity of this expansion is limited and the global heat flux range has to be divided into at least two domains. The first domain corresponds to high

incident heat fluxes where the ignition temperature ($\overline{T}_{ig}$) is attained very quickly, $\overline{t}_{ig} \to 0$, and the second domain corresponds to incident heat fluxes close to the critical heat flux for ignition (in non-dimensional form: $\dot{\overline{q}}''_{0,ig} \approx 1$) where the ignition temperature ($\overline{T}_{ig}$) is attained very slowly, $\overline{t}_{ig} \to \infty$. The fast and long time approximations lead respectively to:

$$\overline{t}_{ig} = \frac{\pi}{4}\frac{1}{(\dot{\overline{q}}''_e)^2} \quad \text{and} \quad \overline{t}_{ig} = \frac{1}{\pi}\left(\frac{1}{1-1/\dot{\overline{q}}''_e}\right)^2 \tag{5}$$

The parameters of the model are obtained from the measurement of the surface temperature of the fuel by a thermocouple and the relationships derived from the Taylor series expansion [46]. A full description of the procedure applied to pine needles can be found in [47] and will not be detailed here. The conductive term in Eq. (1) is assumed to represent radiative transfers through the fuel bed, which can be approximated as a diffusive transfer [47].

b) Porous Fuel Model

The main assumption used to set the model is to consider a thermal equilibrium between the solid and gas phases. This assumption can be questioned, particularly before ignition, and a short discussion about its validity can be found in [50]. Porosity of the fuel bed was also explicitly included by way of $\alpha_s = 1 - \alpha_g$, defined as the volume percentage of the solid phase. The absorption of radiation in the gas phase due to the presence of pyrolysis gases was neglected. In-depth radiation was taken into account to represent the impact of the external heat flux through the porous matrix [51] and the model is expressed as:

$$\alpha_s \rho_s c_{ps} \frac{\partial T}{\partial t} + \alpha_g \rho_g c_{pg} V_{g,x} \frac{\partial T}{\partial x} = k_R \frac{\partial^2 T}{\partial x^2} + \dot{\overline{q}}''_e K e^{-Kx} \tag{6}$$

with the following boundary conditions:

$$x = 0\ ,\ -k_R \frac{\partial T}{\partial x} = h_T\left(T(0,t) - T_\infty\right),\ \underset{x \to \infty}{t = 0} \quad T = T_\infty \tag{7}$$

with ρ_s and ρ_g being the pine needles and the gas densities, respectively; c_{ps} and c_{pg} being the pine needles and gas heat capacities, respectively; $V_{g,x}$ being the gas velocity in the x direction; k_R being the diffusive transfer due to radiation and K being the extinction coefficient of radiation. The value of h_T was kept identical to the previous value used for the solid model (h_T = 22 kW/m^2). An estimation of the radiative and convective transfers at the interface for T_{ig} provided a very close value (less than 20% difference by assuming the needles to be cylinders). In addition to the properties provided in section 2.2, the density was taken as ρ_s = 789 kg/m^3, the thermal capacity as c_{ps} = 3,100 J/kg K and the absorptivity as a_s = 1 [52, 53].

The diffusive transfer in Eq. (6) was assumed to be driven by the radiative transfer through the porous fuel bed [54], while the high value of porosity allowed the neglect of the conductive transfer. The radiative transfer was linearized using the Rosseland approximation:

$$k_R = \frac{16}{3K} B T^3 \quad (8)$$

With B being the Stefan-Boltzmann constant.

3.3. Results and discussion

a) Estimation of the model parameters

Concerning the solid fuel model, the dimensional value of the critical flux for piloted ignition was measured to be $\dot{q}''_e = 8.5\,kW/m^2$ for *Pinus halepensis*. The parameters of the model were obtained from the 0% basket data [47] and are displayed in Table 3. The ignition temperature found in literature for pine needles is between 280-350°C [52]. An estimation of "$k\rho C_p$" from the literature [52, 53], and assuming that the conductivity of heat inside the fuel bed is mainly due to a linearized radiative transfer (as it will be detailed in the next section), provides a value of 0.0755 $(kW/m^2K)^2$ s. These values are different from the values obtained in Table 3, particularly for "$k\rho C_p$". This effect has already been discussed in the literature and it should be noted that the values of the parameters do not represent the actual physical values but the values of the control parameters of the system (see [29] for a full discussion about $k\rho C_p$). However, the estimated parameters are in the range of the physical parameters, and the two sets of parameters exhibit the same discrepancies as for solid fuels [55].

Table 3. Estimated material properties from ignition tests as obtained from the ignition delay times.

Material	$k\rho C_p$ $(kW/m^2K)^2s$	h_T (W/m^2K)	T_{ig} (°C)	t_c (s)	$\dot{q}''_{0,ig}$ (kW/m^2)
Pinus halepensis bed	0.136	22	412	230	8.5

b) Numerical implementation of the porous fuel model

The partial differential equation (Eq. 6) has been numerically integrated on a uniform grid by using a finite volume approach. Diffusive fluxes and convective fluxes have been approximated at the volume interfaces by using central difference and up-wind schemes, respectively. Time advancing has been implemented by using a fully implicit scheme because of its unconditional stability for any time step size. The non-linearity introduced by the Rosseland approximation of the diffusive transfer (Eq. 8) has been treated implicitly; in particular, for each time step, inner iterations are performed until the convergence of the computed temperature field is observed. Spatial and temporal discretization errors have been estimated by using Richardson extrapolation [56]. The spatial discretization error for the adopted space step equal to $1.5 \cdot 10^{-5}$ m has been found to range between 0.20% and 0.35%, depending on the external heat flux. The temporal discretization error for the adopted time step equal to 0.1 s has been found to range between 0.41% and 0.06%, depending on the external heat flux.

It should be noticed that the model is very sensitive to all the physical parameters and particularly to the ignition temperature, which is not a well-defined quantity [29]. However,

the parameters used in this study have only been extracted from measurements [47, 48]. The radiation attenuation has been estimated as detailed in section 2.3 ($K = 170$ m^{-1} and $\delta = 5.88$ mm).

c) Comparison model/experiments

Figure 5 shows the variations of the non-dimensional ignition delay time with non-dimensional external heat flux. Among the 52 experiments for no flow conditions, some provided exactly the same time to ignition, and 14 of them were discarded as aberrant.

The closed baskets (0% opening) display a good agreement with the solid fuel model (Eqs. 1-5). This result is almost unexpected as the assumptions of the solid model were strongly challenged (multiphase medium, surface temperature, conductive transfer through the fuel bed and radiative boundary condition). However, it seems that the prevention of convective transfer in the fuel samples allows for matching the theory. This means that, even if the particles are thermally thin, the bulk properties of the sample induce an equivalent behavior to solid fuels. The samples used for this study are representative of forest floors and the radiative transfer through the porous fuel bed behaves like the conductive transfer through a solid. This result is consistent with the strong radiation attenuation measured for the fuel beds (see section 2.3).

Open baskets show a different behavior. Under natural convection, the ignition times are slightly lower than the ones of the closed baskets for low fluxes, but the difference is not significant. For high fluxes, the buoyancy induced by the quick heating of the surface of the samples does not seem to influence the times to ignition. In this case, the difference in the times is even lower as the sampling rate of the FPA is 1 Hz. Indeed, because of the inverse square root used to present the time results, the scattering induced by a difference of 1 s is low for low fluxes (long times to ignition) and high for high fluxes (short times to ignition). For instance, the two values of the times for a heat flux of 50 kW/m^2 ($\dot{\bar{q}}''_e = 5.88$) correspond to 7 and 8 s, respectively.

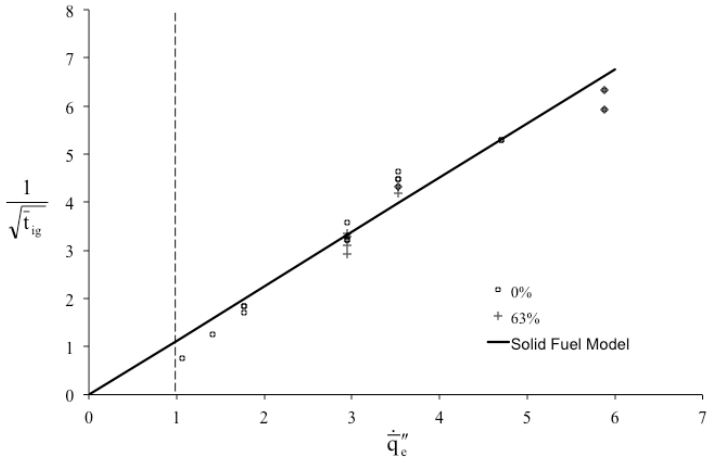

Figure 5. Experimental and modeled ignition delay times vs. the external heat flux for the solid fuel model.

Figure 6 displays the results of the porous fuel model. The first test of the model was conducted for the no-flow conditions. Figure 6 shows that the experimental tendency is well

represented. In-depth radiation allows for taking into account the inflexion in the decrease of the ignition time, as seen for the 0 % baskets opening. The porous model is able to represent the low fluxes, whereas the solid fuel model was obtained for high fluxes (Eq. 5 for high fluxes) and was not accurate for low fluxes. The second test included cooling with a 100 l/mn airflow at the bottom of the basket. The configuration of the FPA does not ensure that all the flow is going through the fuel sample. Thus, $V_{g,x}$ was set to a constant value based on Particle Image Velocimetry measurements [49]. The upward velocity value of 50 mm/s was set in Eq. (6), whatever the experimental conditions. The experimental tendency is matched for low heat fluxes but not for high fluxes. This discrepancy is certainly due to the mixing effect of the pyrolysis gas with air around the pilot flame. This effect has been observed for solid fuels [29, 47] and it is enhanced by the very porous fuel used here and the flow conditions as noted in the previous section.

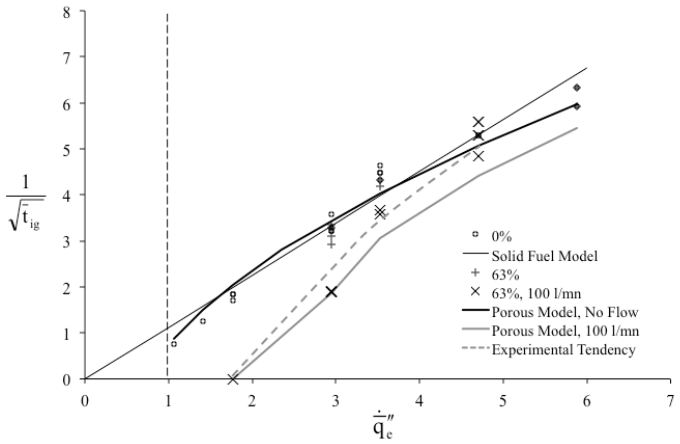

Figure 6. Experimental and modeled ignition delay times vs. the external heat flux for the porous fuel model for all flow conditions.

Furthermore, the flow effect could be different for low and high fluxes, explaining the changing in tendencies compared to the no-flow conditions - the times being longer for low fluxes (see $\dot{q}''_e = 2.94$) and at least equivalent for high fluxes (see $\dot{q}''_e = 4.71$). Indeed, it has been visually observed with low fluxes that the smoke produced by the pyrolysis of the fuel was quite light. The addition of airflow through the fuel bed would increase the fuel lean conditions around the pilot and further delay the ignition. In contrast, the smoke was very dense for high fluxes ($\dot{q}''_e = 4.71$ and 5.88), and the mixing of air with the pyrolysis gases in the surroundings of the pilot flame would decrease the fuel rich conditions towards stoichiometry and shorten the ignition time. This effect is related to the mixing time [45, 46], which has been neglected in both the solid and the porous models and is further investigated for the *Pinus Strobus* experiments.

Figure 7 presents the experimental results with *Pinus Strobus* and the blockage device. For the 0% open baskets, the sample behaved in a solid-like manner, as shown by the linear trend. This result corroborates the results obtained with *Pinus halepensis*. For the 63% open baskets, two flow conditions were investigated - low flow with 50 l/mn and high flow with 100 l/mn. This last condition is higher than the 200 l/mn previously used for *Pinus halepensis* as estimated by PIV [49]. The results for both flow conditions show an increased ignition time

for low heat fluxes. For high heat fluxes this behavior changes, as ignition times for the two flow conditions converge with the ignition times for no flow conditions. The region of convergence is around 40 kW/m^2. At this point radiation from the heat source becomes very high and renders the convective cooling negligible. Under certain conditions faster ignition is observed compared to no flow conditions.

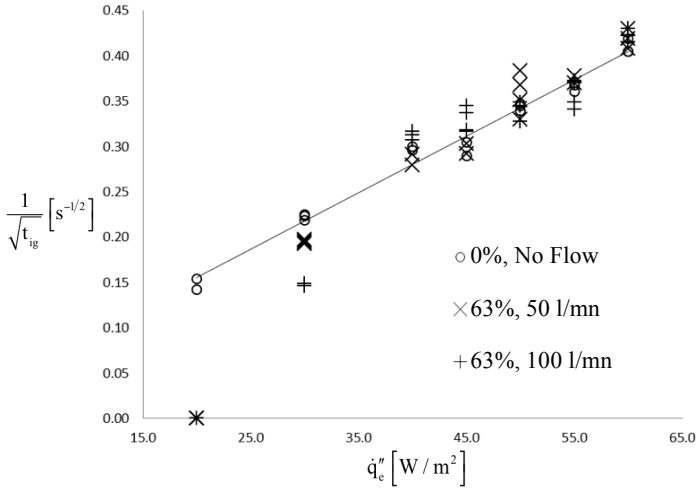

Figure 7. Ignition experiment results for *Pinus strobus* needles.

A likely explanation is that a stoichiometric mixture is formed faster due to the higher pyrolysis rate caused by high heat fluxes coupled with the oxygen transfer from the forced flow. For low heat fluxes (low pyrolysis gas production rate) the forced flow has a negative (increasing the time to ignition) influence as it dilutes the mixture with too much oxygen. For high heat fluxes (high pyrolysis gas production rate) the dilution has a positive (decreasing the time to ignition) quality as a stoichiometric mixture is formed quickly.

Conclusively, the influence of the flow on the time to ignition of porous pine needle litter samples can be observed in the heat transfer as well as the gas transport. It is a constant negative influence for the heat transfer via thermal cooling for low and high heat fluxes. However, for the formation of a stoichiometric mixture it is changing its quality for low and high heat fluxes from negative to positive. This behavior was not observed for *Pinus halepensis*, maybe due to the fact that the highest heat flux was only set up to a lower value of 50 kW/m^2. This effect needs to be further investigated before drawing further conclusions.

The ignition temperature data is used as a second means to obtain the ignition delay time. Additionally, Fig. 8 shows that the average ignition temperature changes with increasing flow magnitude. This is an indication that more energy is needed to ignite the sample when airflow is forced into the sample. The experimental variability was quite high for different repetitions of the same experimental conditions, so these results need to be confirmed in the future. However, it is well known that the ignition temperature is not a constant and varies with the conditions [29], but a constant temperature is still used in recent fire spread models [4, 5, 41].

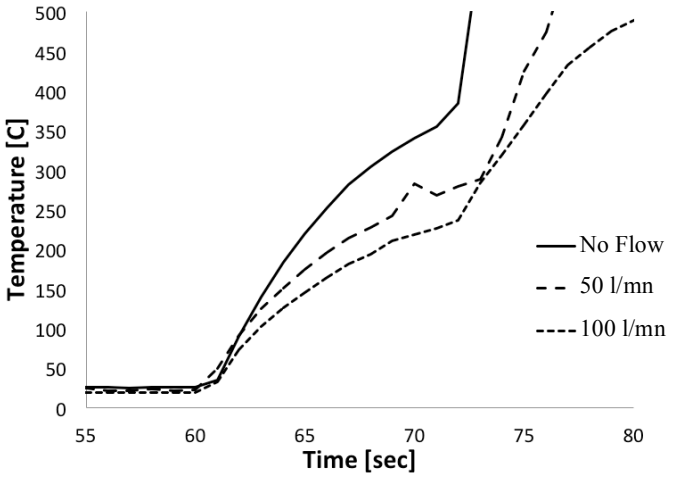

Figure 8. Temperature at the surface of the fuel sample for *Pinus strobus* needles and different flow conditions with a 63% opening basket.

3.4. Solid fuels

a) Modeling considerations

The classical approach to ignition was described in section 3.2.a (Eqs. 1 to 5). A similar, but slightly more complex, expression can be obtained if the same approach is followed with a variable external heat flux $\left(\dot{q}''_e\right)$. Here, the solution of the differential equation will involve additional terms of varied complexity. The simple case of a linear ramp ($\dot{q}''_e = m\,t$, m being a constant) can provide a realistic representation of the heating process generated by external flames and allows the determination an analytical solution similar to Eq. (4). Eq. (5) shows a linear dependency of $1/\sqrt{t_{ig}}$ with $\dot{q}''_e$ (that is the same for the dimensional quantities), independent of the fuel and for a wide range of experimental conditions [57]. If it is assumed that this functional dependency between external heat flux and time is valid, integration over time shows that time scales with $\left(\int_0^t \dot{q}''_e\,dt\right)^2$. This dependency can be readily demonstrated if $\dot{q}''_e$ is a constant, but its validity for a time evolving external heat flux remains to be tested. If time can be scaled by $\left(\int_0^t \dot{q}''_e\,dt\right)^2$, the surface temperature and the ignition delay time can be presented, as a function of the integral of the heat insult, as a single curve that can be used to completely decouple the solid and gas phases in the numerical modeling of the ignition process. This would increase the accuracy without increasing the computational power required.

b) Results and discussion

The tests were conducted with three different materials. These materials (PA6, PA6 with ceramic Nano-fillers, and PMMA) were chosen to represent novel strategies for flammability control by the addition of nano-composites into solid fuels. 36 samples were tested. The tests conditions are described in section 2.1 and the fuels in section 2.2. A quartz tube was used to isolate the combustion area of the FPA. Temperature measurements were obtained from the

thermocouples located in the fuel sample and in the aluminum block. Further description of the experiment is available in [30].

When using the above-described ramp, it is important to prove that the theoretical expressions have validity beyond the integral parameter that is the ignition delay time. Thus, a series of in-depth temperature distribution measurements will be discussed first. The in-depth temperature heating of the sample is presented in Fig. 9 for two sets of times. Figure 9a represents the initial heating of the sample. During this period the inert heating assumption applies well and an increase in temperature close to the surface is observed. This temperature increase decays in-depth, but no signs of endothermicity can be seen. As time evolves (Fig. 9b), the surface reaches the pyrolysis temperature and signs of endothermicity become obvious with no further temperature evolution over time. While the basic assumption of the analytical expressions is challenged [45], this period is close to ignition, thus endothermic pyrolysis will have a weak effect on the ignition characterization. Identical curves were obtained for all other tests conducted but are not presented here.

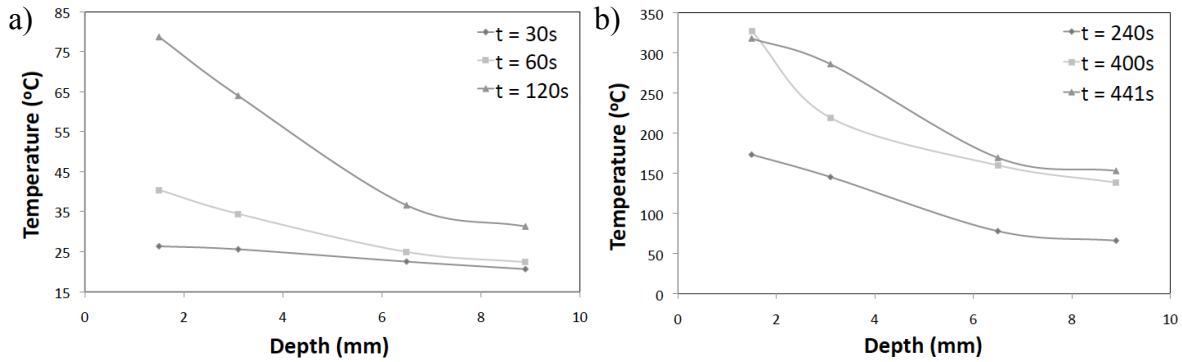

Figure 9. a) Initial heating b) Later heating showing the onset of pyrolysis, for of the PA6 sample.

Figure 10 corresponds to the ignition delay time for the ramp. The heat flux on the abscissa axis corresponds to the average heat flux provided by the ramp (total flux divided by the time to ignition). The time axis is again presented as $1/\sqrt{t_{ig}}$ (see Eq. 5 for high fluxes). The dependencies in the analytical solution for a ramping heat flux are very similar to those obtained for the constant heat flux, thus it can be assumed that the proportionality will remain. However, in this case the Taylor series expansion that leads to Eq. 5 for high fluxes cannot be performed because the heat flux ramps from zero, thus the high heat flux assumption cannot be made and the error functions have to remain.

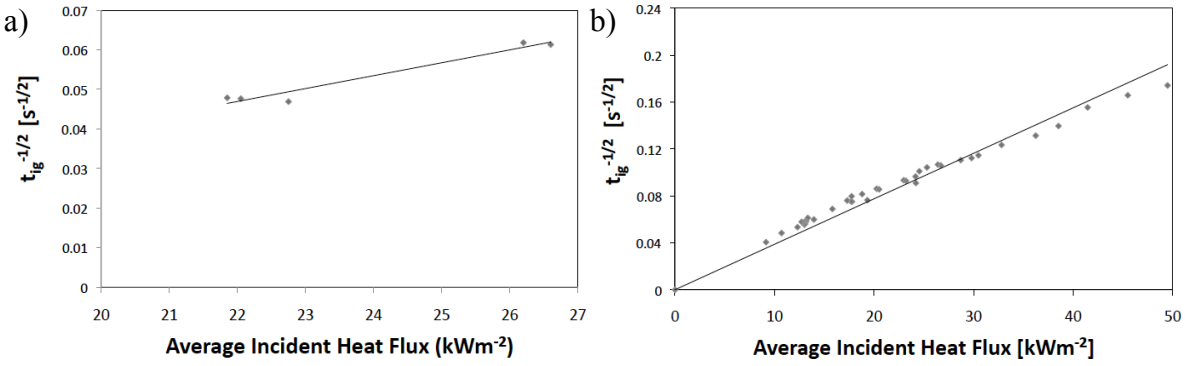

Figure 10. Ignition delay times as a function of the averaged external heat flux (ramping) for a) PA6 and m = 0.1 kW/m^2 s b) PMMA and m = 0.01-5.0 kW/m^2 s.

Figures 11a and b show the dependency of ignition delay time with $\left(\int_0^t \dot{q}''_e \, dt\right)^2$. Again, the behavior is similar to the constant heat flux case, showing that time can effectively be scaled by $\left(\int_0^t \dot{q}''_e \, dt\right)^2$ for a linearly growing heat flux. However, due to the fact that the analytical solution for the ramping heat flux case has not yet been found, no expression equivalent to that of Eq. (5) for high fluxes can be obtained at the moment.

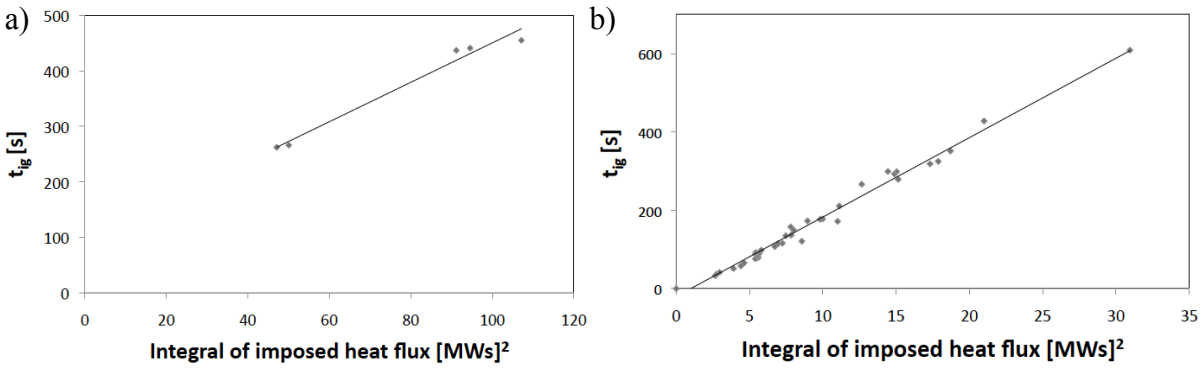

Figure 11. Ignition delay times as a function of the square of the external heat flux (ramping) integrated over time for a) PA6 b) PMMA.

This work provides a realistic approach to the heat flux impacting a structure from a spreading fire by considering an incident heat flux that grows linearly with time. The adaptation of the ignition protocol, utilizing ramping heat flux, on three different materials has shown that the scaling of the time to ignition by $\left(\int_0^t \dot{q}''_e \, dt\right)^2$ is possible. A future step will be to obtain an expression relating the ignition delay time to the incident heat flux for this particular case. This expression, which comes from the analytical solution of the heat diffusion equation with the aforementioned boundary conditions, would completely decouple the solid and gas phase processes and would serve as a tool to predict the time to ignition as a function of a more realistic incident heat flux, thus yielding more accurate results that can be input into forest fire models.

4. Heat Release Rate

The HRR is related to the fire-line intensity [14], which is an important quantity for foresters and fire fighters that allows them to evaluate the fire impact and the means that are required to fight a fire. The fire-line intensity is defined as the rate of heat released per meter of fire front. It can be derived either from the fire rate of spread and the mass loss [14] or from the length of flames [58]. The fire-line intensity of a spreading fire is equal to the HRR divided by the surface area of the sample and multiplied by the depth of the fire front [59]. The fire-line intensity is thus related to the HRR and to the flaming stage of the combustion of

vegetation. As such, it is assumed that a better understanding of the dynamics of heat release during the combustion of fuel samples will allow better estimation of the fire-line intensity.

The first part of this section investigates the influence of the transport processes inside the fuel bed on its combustion dynamics for two different species - *Pinus pinaster* and *Pinus halepensis* [49]. The second section is focused on the influence of species (adding *Pinus laricio* to the two other species) and fuel bulk properties, like permeability and radiation attenuation, on the burning dynamics of forest fuel beds [35].

4.1. Influence of the flow

The HRR was calculated through oxygen consumption calorimetry using O_2, CO_2, and CO values and the classical constant of 13.1 kJ/g of oxygen consumed. The data was highly repeatable within each set of test conditions for the entire test series (see [49]).

Figure 12 shows the HRR estimated in two different ways for given conditions with no-flow and flow. The first HRR estimation was done using oxygen consumption calorimetry, and the second method was done using a smoothed version of the mass loss rate measured during the tests and the heat of combustion of the needles [49]. The experiments performed in the FPA during this test series were well ventilated; only ash remained in the sample basket after test runs (around 0.5 g). The 0% baskets opening had a very small amount of char residue (<0.5 g). Under such well-ventilated and small-scale conditions, the two methods for HRR measurement provided close results. However, the "Heat of Combustion" curves overestimate the "Calorimetry" curves at the first stage of combustion and underestimated them after this point. This behavior could be due to different heats of combustion for flaming and smoldering, the heat of combustion of the pyrolysis gases burned in the flame being lower than that associated with ember creation in the char oxidation process [60]. Thus, using a mean value for the heat of combustion overestimates the HRR during flaming combustion and underestimates it during char oxidation.

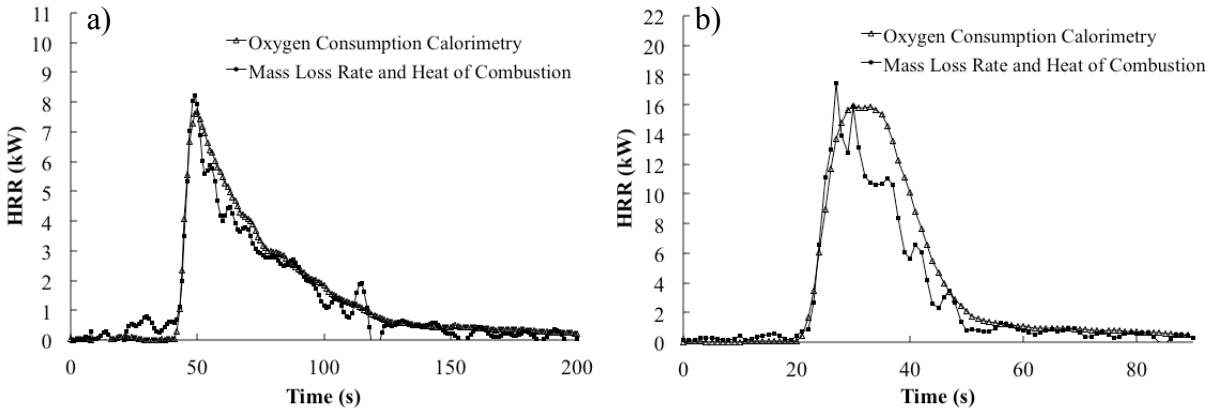

Figure 12. Mean HRR by oxygen consumption calorimetry and mass loss for *Pinus halepensis* and a 26% basket – a) no-flow b) flow.

Figure 13 contains the HRR curves for all of the tests, including both types of needles. Fig. 13a shows the no-flow condition and indicates that the peak HRR was reached at approximately the same time, independent of species and the basket opening. The magnitude of the HRR was affected by the basket opening, with the 63% open basket having the highest value and the 0% open basket having the lowest HRR. This tendency was stronger with *Pinus*

halepensis and attributed to the higher surface-to-volume ratio (see section 2.2). This parameter affected the internal fuel bed and impacted thermal transfers and surface area for contact with oxygen. *Pinus pinaster* also exhibited a higher HRR for a given flow condition. Fig. 13b shows the HRR estimate for the flow conditions, indicating that the flow has an effect on both the time to reach peak HRR and the magnitude of the HRR. The tendencies are reversed for peak HRR, and *Pinus pinaster* exhibited an influence of the basket opening on the time to reach peak HRR. This effect could be due to the changing in the inlet flow through the fuel bed, as the needle beds are less dense and cooling by fresh air was allowed. With *Pinus halepensis*, as the flow was driven by the dense fuel bed, the basket opening has no effect.

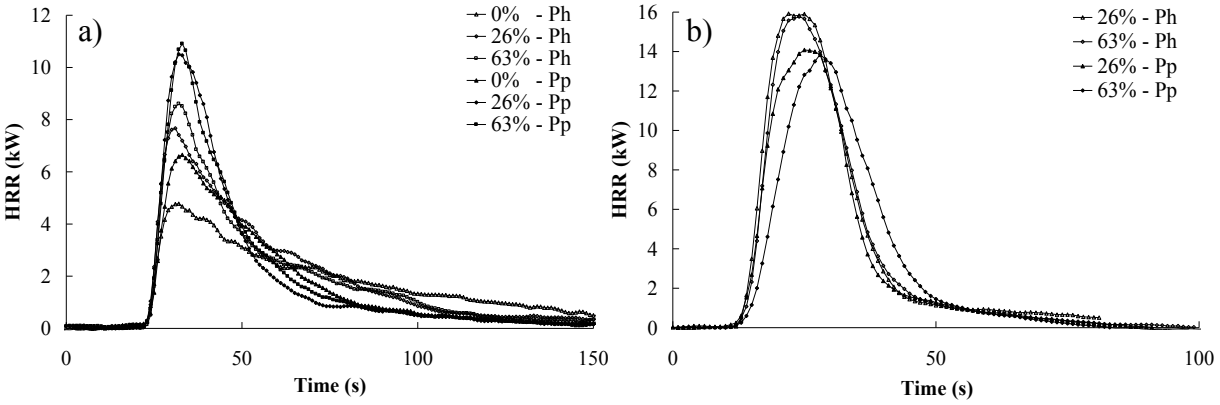

Figure 13. Mean heat release rates for the different baskets with *Pinus halepensis* (Ph) and *Pinus pinaster* (Pp) – a) no-flow b) flow conditions.

Figure 14 presents CO_2 and CO production for different test conditions and demonstrates the changing in behavior of the combustion process. The vertical lines indicate the minimum and maximum (dashed) times, as well as the mean (solid) time to flameout for the test runs. The results are discussed using the measured data of the time curves and visual observations made during the tests. CO concentration is a good indicator of the fuel bed behavior with respect to the dynamics of flaming versus glowing combustion.

Fig. 14a illustrates no-flow and 0% basket opening conditions. The CO_2 curve reflects a long duration for flaming combustion (around 130 s). When correlated with the observations, the CO curve provides insight to the different steps involved in the combustion of the fuel samples. The first steep increase was due to the ignition of the sample on the upper surface. A steady production of CO follows. During this step, the burning front spread from the top to the bottom of the basket. As the basket was closed, air could only come from the top of the fuel sample. It was consumed at the surface of the bed by the flame and the superficial char. Thus, the reaction was slow with low observed flames and a propagation of the pyrolysis front from the top to the bottom of the bed during combustion. When this spreading ended, no more degradation gases were produced and the flame extinguished. Then, oxygen was able to reach the surface of the remaining charred material and combustion of embers within the fuel bed started. The last decrease in the CO curve corresponded to the extinction of all combustion in the sample.

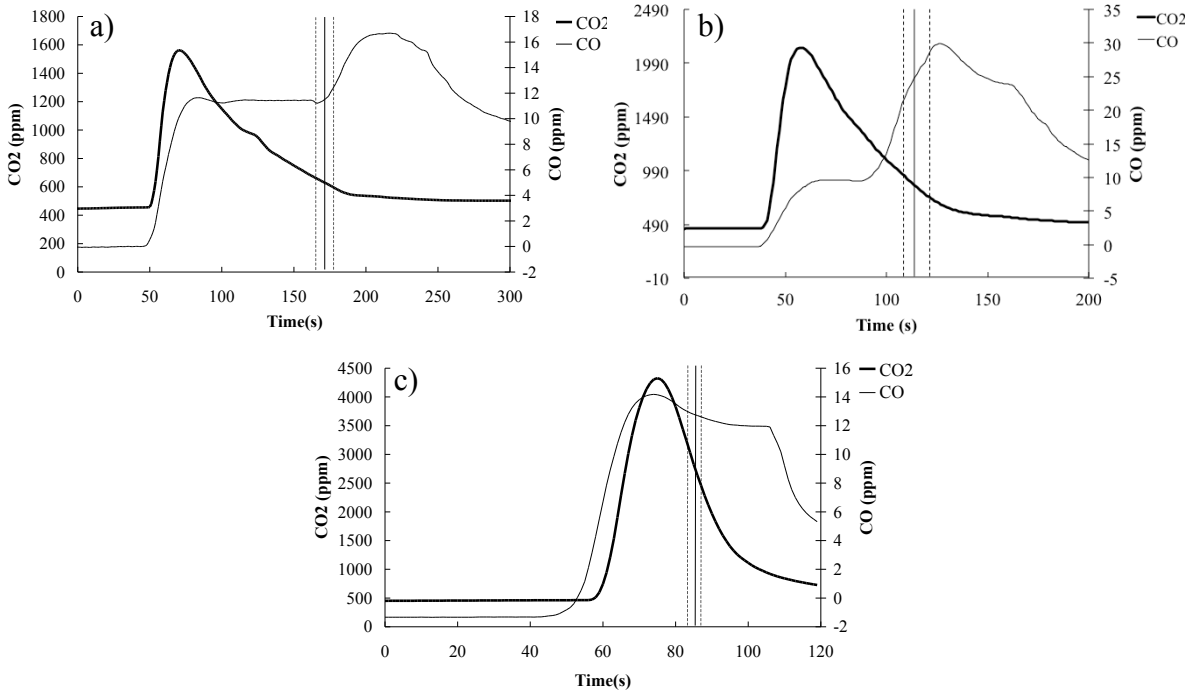

Figure 14. Mean CO_2 and CO concentrations for *Pinus halepensis* needles – a) no-flow and 0% opening b) no-flow and 26% opening c) flow and 26% opening.

Figure 14b corresponds to natural convection, as the bottom of the bed was ventilated due to the open basket. At the ignition point both CO_2 and CO generation rates increased. As the fuel was consumed, greater amounts of char and ash were formed. The flame decreased toward extinction and the CO_2 generation rate peaked and then decreased rapidly. CO generation became constant during the flame regression stage. As smoldering combustion proceeded, the CO production increased close to flameout and then fell off until the embers extinguished. The steady step was shorter than the one for closed basket conditions (Fig. 14a), and corresponded to only flaming combustion because the flame consumed the oxygen before it could reach the fuel bed. The short steady step and the two slopes in the consecutive increase of CO (before and after the line representing flame extinction) are mainly due to the overlap between flaming and char combustion when the flame was decreasing. The combustion of embers started on the edges of the fuel sample before flameout, leading to an increase in CO production.

Figure 14c describes the 26% basket opening and flow conditions. The CO_2 curve demonstrates a short duration of combustion (around 40 s). The steady state disappeared. We observed a fast phenomenon with embers starting to burn before the completion of the flame spread through the fuel bed. This behavior was mainly due to the additional oxygen supplied inside the fuel bed by the forced flow. It demonstrates that flaming and smoldering occurred simultaneously. Current fire-spread models either neglect smoldering [7] or assume that it happens consecutively for the same particle [4, 41]. The results suggest that the separation between smoldering and flaming should be further investigated under flow conditions.

CO concentration profiles proved to be good indicator of the dynamics of the combustion process. The transition between flaming combustion and glowing embers was reflected in the measured CO responses. Again, the ability for combustion air to flow into the porous bed

allowed the measured CO concentrations to provide good data on internal fuel bed dynamics. The pine needle species studied behaved differently due to different packed densities and different surface-to-volume ratios. The following section is devoted to the analysis of these last influences to developing a better understanding of the burning dynamics of the porous fuel beds.

4.2. Influence of the fuel properties

The previous section has shown that flow conditions through the porous fuel bed and fuel species have both an influence on the burning dynamics of pine needles and develop cross interactions [48, 49]. However, these studies did not discriminate between these effects and did not study the main bulk property of porous fuel beds, which is permeability. The different parameters playing a role on the oxygen supply inside the fuel bed (i.e. flow magnitude and fuel bed permeability) as well as the influence of fuel species properties are studied in this section. This section also represents a further step towards improving wildland fire spread models by estimating the influence of fuel and fuel bed properties on quantities such as the mean heat released during flaming.

The HRR has been better estimated by improving the estimation of the calorimetric constants for each fuel species from the fuels ultimate analysis and Low Heating Values [61]. This allows enhancing the comparison between pine species as they have different calorimetric constants [35].

a) *Fuel bed properties*

In the previous section, the air supply was artificially controlled by the basket opening and the forced flow. Under actual fire conditions, the oxygen supply will be controlled by the permeability of the porous medium and the flow magnitude inside the fuel bed. Thus, permeability experiments have been performed with *Pinus halepensis* for different permeability values and flow conditions [35] (see section 2.4). The study has been focused on the flaming stage, as this stage is mainly responsible for the fire spread.

The results are presented in terms of mean HRR divided by the fuel mass loss during the flaming stage ($kW.g^{-1}$). This quantity can be seen as a mean heat of combustion (because it is constant over time) and is close to the definition of the fire-line intensity used for wildfires [14, 58].

Figure 15 shows the results obtained for *Pinus halepensis* with four different values of the fuel bed permeability. The vertical bars represent the experimental variability. There is no experimental data for the higher permeability with High Flow (HF: 200 l/mn) since it was impossible to obtain a piloted ignition. Some results are quite scattered since the ignition time was quite sensitive to the surrounding flow. For a given condition (basket and flow) the energy released during the combustion of the porous fuel bed increases with its permeability. Indeed, the oxygen supply inside the porous fuel bed is enhanced with increasing permeability. It can also be seen that the flow influence increases with the permeability as the slopes of the curves increase with it. Porous fuel beds permeability influence on forest fuel combustion dynamic appears to be important and should be taken into account when modeling fire spread in such fuel beds. The experimental tendencies could not be explained only by porosity, which is less representative of the influence of the flow than permeability. The interested reader is referred to [62] for more discussion about the effects of permeability and porosity and how they are related to each other.

The HF values show an inflexion in the increase tendency. It looks as if the flow enhancement of the burning is reaching a limit. However, the HRR is still increasing greatly between Low Flow (LF: 100 l/mn) and HF [35]. A misleading conclusion could be reached because of analyzing only a mean value. It highlights the limitations in the use of mean values like the fire-line intensity in wildfires. The mean values can lead to an underestimation of the peak values of energy released during a fire and need to be used with other instantaneous quantities [35]. The increase of the HRR with permeability for a given flow condition can be explained by the increase of the free mean path of radiation. The surface-to-volume ratio of the needles is a constant for a given species, and the mean free path of radiation increases with the permeability of the fuel bed, increasing the in-depth heating of the fuel sample. As more fuel is heated up, the pyrolysis rate and the burning of the samples are enhanced.

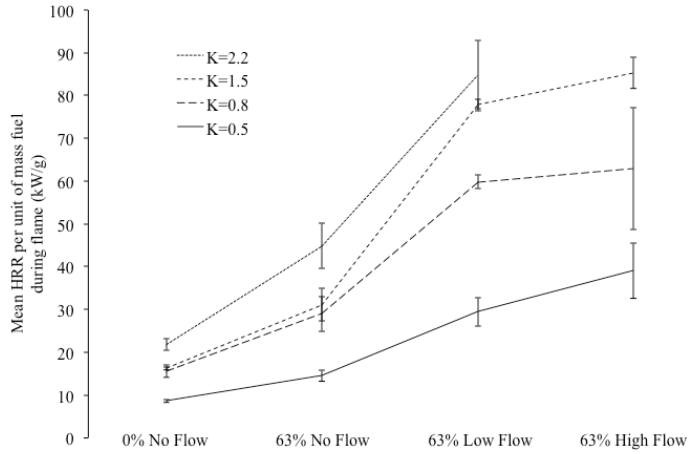

Figure 15. *Pinus halepensis* mean HRR per unit of fuel mass during the flame as a function of the permeability K (10^{-7} m^2).

b) *Fuel species*

The three species have different geometrical and chemical characteristics [53] as well as different values of permeability for the same sample mass (see Table 2). To remove the influence of the fuel beds on the flow, a set of experiments has been performed with the same permeability of $1.5.10^{-7}$ m^2 for the three species. The mass of fuel used has been estimated from the permeability data (see Table 2), providing 12, 13 and 15 g for *Pinus halepensis*, *Pinus laricio* and *Pinus pinaster*, respectively.

The three species present different combustion dynamics, with different flame durations and mass losses during flaming. These two quantities increase with the surface-to-volume ratio of the species [35]. The influence of species has been analyzed, as was done previously, and is presented in Fig. 16. The curves merely represent polynomial trend lines between the experimental data points. Under no flow conditions the heat released by the three species during flaming increases when more oxygen is allowed to pass through the fuel bed sample. *Pinus halepensis* and *Pinus laricio* display close values. *Pinus pinaster* seems to be more "energetic" than the two others species but it has the lowest lower heating value [34]. Thus, the chemical properties of the species cannot explain this result. The difference between species may be due to the radiative transfer inside the fuel bed, as described previously, or due to the fact that this species (*Pinus pinaster*) is releasing the highest amount of flammable gases during pyrolysis [63]. Under flow conditions the tendency is changing. For *Pinus halepensis*

and *Pinus laricio* the heat released per unit mass increases with the flow. *Pinus halepensis* is more influenced by the flow than *Pinus laricio*, maybe because of its high surface-to-volume ratio that allows more oxygen contact at the surface of the solid for pyrolysis and heterogeneous reactions. However, there is an inflexion for the two species when a high flow (HF) is applied. For *Pinus pinaster*, the mean HRR per unit mass is decreasing. The same cooling limiting effect as the one observed in Fig. 13b has been observed for *Pinus pinaster*. Some limiting effects are even likely to occur when increasing the flow further, such as the dilution of the pyrolysis gases as stated for ignition (section 3). It seems that the oxygen supply is already sufficient with the low flow and that increasing the flow slows down the reaction. As no significant changes have been noticed in CO, CO_2, or soot production between low flow and high flow conditions, this result is not attributed to a change in combustion regime. It could be due to a change in the pyrolysis process under high flow conditions, due to the increased presence of air. It could also be due to the thickness of the needles (low surface-to-volume ratio) and the low contact surface available for heterogeneous reactions compared to the other species. This effect needs to be further investigated in the future.

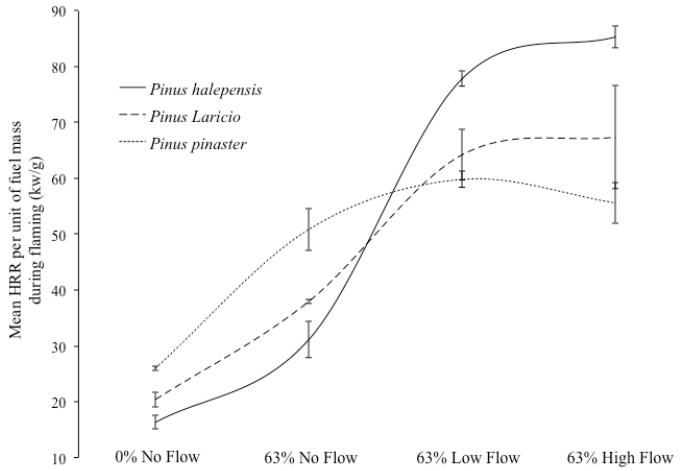

Figure 16. Mean HRR per unit of fuel mass during the flame for the three species, $K = 1.5.10^{-7}\ m^2$.

This study showed that permeability is one of the main bulk parameters driving the burning dynamics of porous fuel beds, along with the free mean path of radiation. However, for a given permeability, the different fuel species have a varying influence on the HRR. This influence seems to be mainly due to the physical properties of the fuels as the fuels have very close lower heating values. Only *Pinus pinaster* displays a different behavior, which could be fuel specific and needs to be further investigated. The description of the burning dynamics cannot rely only on mean quantities. In the future, the HRR needs to be quantified as a function of permeability and mean path of radiation.

5. Conclusions

This paper represents the flammability studies related to wildland and WUI fires that have been conducted at the University of Edinburgh and at WPI over the last 5 years. The whole approach is based on experiments conducted with the Fire Propagation apparatus and modified protocols were applied to meet the needs of each different study. The techniques presented

here are not new in fire science, but their application and adaptation to the wildland fire problem is innovative and shows promising results. The results can be summarized as follows:

- *Time to ignition:* Concerning the pine needle beds, experiments and modeling have been used to understand the processes involved in porous wildland fuel ignition. Under no flow conditions and despite thermally thin pine needles, the bulk properties of the fuel bed (radiation attenuation) induced a solid-like behavior. Under flow conditions, the tendency was different and a porous fuel model has been developed to take into account the effect of cooling in the fuel layer due to forced flows. It allowed matching the experimental conditions for low flow but not for high flow. This result is likely to be due to the condition of mixing of pyrolysis gases with air around the pilot flame. An additional experimental study with *Pinus strobus* showed that competing thermal and mixing effects were involved.
  Concerning solid fuels, an experimental study was conducted to provide a realistic heating condition by considering an incident heat flux, which grew linearly with time. The experiments under these novel testing conditions on three different materials showed that the scaling of the time to ignition by $\left(\int_0^t \dot{q}''_e \, dt\right)^2$ is possible. An expression relating the ignition delay time with the incident heat flux for this particular case is yet to be obtained. It would allow a full decoupling of solid and gas phase processes, yielding accurate results that can be input into forest fire models.
- *Heat release rate:* Regarding the influence of the flow, the results indicate that the transport processes inside the bed have a significant impact on the combustion process within the porous fuel bed. The HRR calculated by means of calorimetry was reinforced by the use of mass loss rate and heat of combustion in the well-ventilated test conditions. CO concentration profiles proved to be a good indicator of the dynamics of the combustion process. The pine needle species studied behaved differently due to different packed densities and different surface-to-volume ratios.
  Regarding the influence of the fuel properties, the results showed that permeability is one of the main parameters driving the burning dynamics of porous fuel beds. Another important bulk property is the free mean path of radiation. The results also showed that, for a given permeability, the fuel species have an influence on the HRR but that this influence seems to be mainly due to the physical properties of the fuels and not the chemical ones. Only *Pinus pinaster* displayed a different behavior, which could be fuel specific and needs to be further investigated.

These first results improved our understanding of how porous fuel beds and solid fuels ignite and burn under conditions related to wildland and WUI fires. However, these studies are only the gateway to a new field of investigation, and the next important step will be to find the ways to quantify the role of the different parameters in order to improve the ability of wildand fire spread models to describe vegetation burning and structural ignition.

Acknowledgement

The authors would like to thank Nicolas Bal, Hubert Biteau, Thomas Steinhaus, Paolo Fiorucci and Chris Schemel for helping with the experiments and for the useful discussions. Factory Mutual Global Corporation generously donated the FPAs to the University of Edinburgh and WPI.

References

[1] McArthur, A. G. (1967) "Fire behaviour in eucalypt forest," Department of National Development, Australian Forestry and Timber Bureau, Leaflet 107, Camberra.

[2] Rothermel, R. C. (1972) "A Mathematical Model for Predicting Fire Spread in Wildland Fuels," No. INT-115, U.S. Department of Agriculture, Forest Service, Ogden.

[3] Morvan, D. (2011) Physical Phenomena and Length Scales Governing the Behaviour of Wildfires: A Case for Physical Modelling, Fire Technology, 47(2), pp. 437-460.

[4] Morvan, D., Mèradji, S., and Accary, G. (2009) Physical modelling of fire spread in Grasslands, Fire Safety Journal, 44(1), pp. 50-61.

[5] Mell, W., Maranghides, A., McDermott, R., and Manzello, S. L. (2009) Numerical simulation and experiments of burning douglas fir trees, Combustion and Flame, 156(10), pp. 2023-2041.

[6] Linn, R. R. (1997) "A transport model for prediction of wildfire behavior," Ph.D. Thesis, New Mexico State University, LANL.

[7] Mell, W., Jenkins, M. A., Gould, J., and Cheney, P. (2007) A physics-based approach to modelling grassland fires, International Journal of Wildland Fire, 16(1), pp. 1-22.

[8] Mell, W. E., Manzello, S. L., Maranghides, A., Butry, D., and Rehm, R. G. (2010) The wildland-urban interface fire problem - current approaches and research needs, International Journal of Wildland Fire, 19(2), pp. 238-251.

[9] Deeming J.E., Lancaster J.W., Fosberg M.A., Furman W.R., Shroeder M.J. (1972) The National Fire-Danger Rating System. United States Department of Agriculture, Forest Service, Research Paper RM 84, 165 pages, revised 1974.

[10] Burgan, R.E. (1988) 1988 revisions to the 1978 National Fire-Danger Rating System. United States Department of Agriculture, Forest Service, Research Paper SE-273, 39 pages.

[11] Stocks B.J., Lawson B.D., Alexander M.E., Van Wagner C.E., McAlpine R.S., Lynham T.J., Dubé D.E. (1989) The Canadian forest fire danger rating system: an overview. The Forestry Chronicle, 65, pp. 258-265.

[12] European Forest Fire Information System, EC Joint Research Centre, Institute for Environment and Sustainability – http://effis.jrc.ec.europa.eu.

[13] McArthur, A.G. (1967) “Fire Behaviour in Eucalypt Forest,” Comm. Aust. Timb. Bur. Leaflet 107, 25 pages.

[14] Byram G.M. (1959) “Combustion of forest fuels”. In: Davis KP, editor. Forest fire control and use. New York: McGraw-Hill Book Company, pp. 61-89.

[15] Cordova, J.L., Walther, D.C., Torero J.L., Fernandez-Pello, A.C. (2001) Oxidizer Flow Effects on the Flammability of Solid Combustibles. Combustion Science and Technology, 164(1-6), pp. 253-278.

[16] Babrauskas V., Peacock R.D. (1992) Heat release rate: The single most important variable in fire hazard. Fire Safety Journal, 18(3), pp. 255-272.

[17] SFPE Handbook of Fire Protection Engineering, 4th Edition, 2009.

[18] Chandler C., Cheney P., Thomas P., Trabaud L., Williams D. (1983) Fire in Forestry, vol. 1, John Wiley & Sons, New York.

[19] Pereira J.M.C., Sequeira N.M.S., Carreiras J.M.B. (1995) Structural Properties and Dimensional Relations of Some Mediterranean Shrub Fuels. International Journal of Wildland Fire, 5(1), pp. 35-42.

[20] Catchpole E.A., Catchpole W.R., Viney N.R., McCaw W.L., Marsden-Smedley J.B. (2001) Estimating fuel response time and predicting fuel moisture content from field data. International Journal of Wildland Fire, 10, pp. 215-222.

[21] Dimitrakopoulos A.P., Papaioannou K.K. (2001) Flammability Assessment of Mediterranean Forest Fuels. Fire Technology, 37(2), pp. 143-152.

[22] Liodakis S., Kakardakis T. (2008) Measuring the Relative Particle Foliar Combustibility of WUI Forest Species Located Near Athens. Journal of Thermal Analysis and Calorimetry, 93(2), pp. 627-635.

[23] Valette, J.C. (1990) Inflammabilité d'espèces forestières méditerrannéenes: Conséquences sur la combustibilité des formations forestières. Revue Forestière Française, 42, pp. 76-92.

[24] Dimitrakopoulos A.P., Panov P.I. (2001) Pyric properties of some dominant Mediterranean vegetation species. International Journal of Wildland Fire, 10(1), pp. 23-27.

[25] Catchpole W.R., Catchpole E.A., Butler B.W., Rothermel R.C., Morris G.A., Latham D.J. (1998) Rate of Spread of Free-Burning Fires in Woody Fuels in a Wind Tunnel. Combustion Science and Technology, 131(1), pp. 1-37.

[26] Mendes-Lopes J.M.C., Ventura J.M.P., Amaral J.M.P. (2003) Flame characteristics, temperature–time curves, and rate of spread in fires propagating in a bed of Pinus pinaster needles. International Journal of Wildland Fire, 12(1), pp. 67-84.

[27] Weise D., White R., Beall F., Etlinger M. (2005) Use of the cone calorimeter to detect seasonal differences in selected combustion characteristics of ornamental vegetation. International Journal of Wildland Fire, 14, pp. 321-338.

[28] Dibble, A.C., White, R.H., Lebow P.K. (2007) Combustion characteristics of north-eastern USA vegetation tested in the cone calorimeter: invasive versus non-invasive plants. International Journal of Wildland Fire, 16, pp. 426-443.

[29] Torero J.L. (2009) "Ignition of Solids". The SFPE Handbook of Fire Protection Engineering, (4th ed.), DiNenno P.J. (ed.), National Fire Protection Association, Quincy, MA 02269, p. 2/260.

[30] Borowiec P., Reszka P., Steinhaus T., Torero J.L. (2009) Characterization of ignition by direct radiation from flames for Urban/Wildland applications. 6th Mediterranean Combustion Symposium, Ajaccio, 7-11 June.

[31] Jervis, F., Rein, G., Torero, J., and Simeoni, A. (2010) The Role of Moisture in the Burning of Live and Dead Pine Needles, Proc. 6th International Seminar on Fire and Explosion Hazards, Leeds, UK, 11-16 April.

[32] Manzello, S.L., Suzuki, S and Hayashi, Y. (2012) Enabling the Study of Structure Vulnerabilities to Ignition from Wind Driven Firebrand Showers: A Summary of Experimental Results. Fire Safety Journal, to appear.

[33] "Standard Test Method for Measurement of Synthetic Polymer Material Flammability Using a Fire Propagation Apparatus". (2003) ASTM, E2058-03.

[34] Morandini, F., Simeoni, A., Santoni, P.A., Balbi, J.H. (2005) A model for the spread of fire across a fuel bed incorporating the effects of wind and slope. Combustion Science and Technology,177, pp. 1381-1418.

[35] Simeoni, A., Bartoli, P., Torero, J. L., Santoni, P. A. (2011) On the Role of Bulk Properties and Fuel Species on the Burning Dynamics of Pine Forest Litters, Proc. 10th IAFSS Symposium, University of Maryland, USA, June 19-24.

[36] Thomas, J.C., Simeoni, A., Colella, F., Torero, J.L. (2011) Piloted Ignition Regimes of Wildland Fuel Beds. Fall Technical Meeting of the Eastern States Section of the Combustion Institute, Storr, CT, October 9-12.

[37] Grishin A.M. (1997) Mathematical modeling of forest fires and new methods of fighting them. Publishing House of the Tomsk State University, Albini (ed.), Russia.

[38] Grishin A.M., Zima V.P., Kutznetsov V.T., Skorik A.I. (2002) Ignition of Combustible Forest Materials by a Radiant Energy Flux. Combustion, Explosion and Shock Waves, 38(1), pp. 24-29.

[39] A. Simeoni, F. Colella, E. Martinot, P. Bartoli, J.L. Torero (2010) Flaming ignition of pine needle beds. 6th International Conference on Forest Fire Research, Coimbra, Portugal, 15-18 November.

[40] De Mestre, N.J., Catchpole, E.A., Anderson, D.H., Rothermel, R.C. (1989) Uniform Propagation of a Planar Fire Front without Wind, Combustion Science and Technology, 65(4-6), pp. 231-244.

[41] Porterie B., Morvan D., Loraud J.C., Larini M. (2000) Firespread through fuel beds: Modeling of wind-aided fires and induced hydrodynamics. Physics of Fluids, 12(7), pp. 1762-1781.

[42] Vaz G.C., André J.C.S., Viegas D.X. (2004) Estimation of the Radiation Extinction Coefficient of Natural Fuel Beds. International Journal of Wildland Fire, 13, pp. 65-71.

[43] Kaviany, M. (1995) Principles of Heat Transfer in Porous Media (2nd ed.), Springer, New York, p. 28.

[44] Mendes-Lopes, J.M.C., Ventura, J.M.P., Santos, C.F.P. (2002) Experimental determination of pressure drop through a bed of pine needles, Proceedings of the 4th International Conference on Forest Fire Research, D X Viegas Ed., CD-ROM.

[45] Quintiere, J.G. (1981) A Simplified Theory for Generalizing Results from a Radiant Panel rate of Flame Spread Apparatus. Fire and Materials 5(2), pp. 52-60.

[46] Long, R.T., Torero, J.L., Quintiere, J.G., Fernandez-Pello, A.C. (1999) Scale and Transport Considerations on Piloted ignition of PMMA, Proc. 6th International Symposium on Fire Safety Science, M. Curtat, ed., IAFSS, pp. 567-578.

[47] J.L. Torero, A. Simeoni (2010) Heat and mass transfer in fires: Scaling laws and application to forest fires. The Open Thermodynamics Journal, 4, pp. 145-155.

[48] Bartoli, P., Simeoni, A., Torero, J.L., Santoni, P.A. (2011) Determination of the main parameters influencing forest fuel combustion dynamics. Fire Safety Journal, 46(1-2), pp. 27-33.

[49] Schemel, C., Simeoni, A., Biteau, H., Riviera, J., Torero, J.L. (2008) A calorimetric study of wildland fuels. Experimental Thermal and Fluid Science, 32(7), pp. 1381-1389.

[50] Simeoni, A., Santoni, P.A., Larini, M., Balbi, J.H. (2003) Reduction of a multiphase formulation to include a simplified flow in a semi-physical model of fire spread across a fuel bed. International Journal of Thermal Science, 42, pp. 95-105.

[51] Jiang, F., de Ris, J. L., and Khan, M. M. (2009) Absorption of thermal energy in PMMA by in-depth radiation. Fire Safety Journal, 44(1), pp. 106-112.

[52] "Deliverable D-02-02: A: Physical, chemical and thermal characteristics of the wildland fuel particles – Answer from the partners" (2004) EUFIRELAB: A Wall-Less Laboratory for Wildland Fire Sciences and Technologies in the Euro-Mediterranean Region, EU FP5 Program EVR1-CT-2002-40028.

[53] Tihay, V., Simeoni, A., Santoni, P.A., Rossi, L., Garo, J.P., Vantelon, J.P. (2009) Experimental study of laminar flames obtained by the homogenization of three forest fuels, International Journal of Thermal Sciences, 48(3), pp. 488-501.

[54] Bouma, P.H., De Goey, P.H. (1999) Premixed Combustion on Ceramic Foam Burners, Combustion and Flame, 119, pp. 133-143.

[55] Mowrer, F.W. (2005) An Analysis of Effective Thermal Properties of Thermally Thick Materials. Fire Safety Journal, 40, pp. 395-410.

[56] Ferziger, J.H., Peric M. (2002) Computational methods for fluid dynamics (3rd ed.), Springer, Berlin, Germany, p 59.

[57] Atreya, A. (1998) Ignition of Fires. Philosophical Transactions Royal Society London A, 356, pp. 2787-2813.

[58] Alexander, M.E. (1982) Calculating and interpreting forest fire intensities. Canadian Journal of Botany, 60, pp. 349-357.

[59] Finney, M.A. (1998) "FARSITE: Fire area simulator – model development and evaluation," USDA, Forest Service, Rocky Mountains Research Station, Research Paper RMRS-RP-4, Ogden, Utah, 47 p.

[60] Leroy, V., Cancellieri, D., Leoni, E. (2006) Thermal degradation of ligno-cellulosic fuels: DSC and TGA studies. Thermochimica Acta, 451, pp. 131-138.

[61] Biteau, H., Steinhaus, T., Schemel, C., Simeoni, A., Marlair, G., Bal, N., and Torero, J.L. (2008) Calculation methods for the heat release rate of materials of unknown composition, Fire Safety Science – Proceedings of the 9th International Symposium, International Association for Fire Safety Science, pp. 1165-1176.

[62] Bartoli, P. (2011) Forest fires: improvement of the knowledge of the coupling between flames and vegetative fuels, Ph.D. Thesis, University of Corsica and University of Edinburgh, 270 p.

[63] Tihay, V., Santoni, P.A., Simeoni, A., Garo, J.P., Vantelon, J.P. (2009) Skeletal and global mechanisms for the combustion of gases released by crushed forest fuels, Combustion and Flame, 156, pp. 1565-1575.

List of Figures

List of Tables